

# A soft touch with electron beams: Digging out structural information of nanomaterials with advanced scanning low energy electron microscopy coupled with deep learning



Eliška Materna Mikmeková<sup>a</sup>, Jiří Materna<sup>b</sup>, Ivo Konvalina<sup>a,\*</sup>, Šárka Mikmeková<sup>a</sup>, Ilona Müllerová<sup>a</sup>, Tewodros Asefa<sup>c,d</sup>

<sup>a</sup> Institute of Scientific Instruments of the Czech Academy of Sciences, Královopolská 147, 612 64 Brno, Czech Republic

<sup>b</sup> Machine Learning College, s.r.o., Chrlícká 787/56, 620 00 Brno, Czech Republic

<sup>c</sup> Department of Chemistry & Chemical Biology, Rutgers, The State University of New Jersey, 610 Taylor Road, Piscataway, New Jersey 08854, USA

<sup>d</sup> Department of Chemical & Biochemical Engineering, Rutgers, The State University of New Jersey 98 Brett Road, Piscataway, New Jersey 08854, USA

## ARTICLE INFO

### Keywords:

Scanning low energy electron microscopy  
Deep learning  
Mesoporous silica

## ABSTRACT

Nanostructured materials continue to find applications in various electronic and sensing devices, chromatography, separations, drug delivery, renewable energy, and catalysis. While major advancements on the synthesis and characterization of these materials have already been made, getting information about their structures at sub-nanometer resolution remains challenging. It is also unfortunate to find that many emerging or already available powerful analytical methods take time to be fully adopted for characterization of various nanomaterials. The scanning low energy electron microscopy (SLEEM) is a good example to this. In this report, we show how clearer structural and surface information at nanoscale can be obtained by SLEEM, coupled with deep learning. The method is demonstrated using Au nanoparticles-loaded mesoporous silica as a model system. Moreover, unlike conventional scanning electron microscopy (SEM), SLEEM does not require the samples to be coated with conductive films for analysis; thus, not only it is convenient to use but it also does not give artifacts. The results further reveal that SLEEM and deep learning can serve as great tools to analyze materials at nanoscale well. The biggest advantage of the presented method is its availability, as most modern SEMs are able to operate at low energies and deep learning methods are already being widely used in many fields.

## 1. Introduction

Since their inception in the early 1990s, mesoporous materials have been receiving a great deal of attention due to their interesting structures, high surface areas, and nanometer pores (typically 1.5–15 nm) [1–3]. Among many types of mesoporous materials reported so far, MCM41 (Mobil Composition of Matter) and SBA-15 (Santa Barbara Amorphous) constitute the two most widely studied and useful mesoporous metal oxides [4]. Their structures and large surface areas allow them to host a variety of organic and organometallic functional groups, and even enzymes, for (bio)catalysis, electrochemistry, sensing, drug delivery, hydrogen storage, and separation applications [5–9]. For example, MCM-41 and SBA-15 type mesoporous materials were demonstrated to have an ability to adsorb light hydrocarbons or pollutants from gas phase as well as from aqueous solutions for

environmental protection [10–12]. In other reports, metallic nanoparticles and nanowires were hosted within the pores of mesoporous silicas to create materials that are useful for nanoelectronics, plasmonic, and photocatalysis applications [13–15]. The nanopores of mesoporous SBA-15 were also shown to support metallic ions and nanoparticles and form heterogeneous nanocatalysts for various reactions [16–19]. Other reports demonstrated the potential applications of functionalized mesoporous materials for controlled and targeted delivery of drugs in biological systems and for biosensing [6,20,21].

To further improve the properties, for example, the catalytic activity and selectivity, of many of these materials as well as other related nanomaterials, it is necessary to fully understand their structures and surfaces at nanoscale. The outcome can also help the rational design and synthesis of mesoporous materials with better surface structures and desirable properties and performances. However, owing to their beam

\* Corresponding author at: Institute of Scientific Instruments of the Czech Academy of Sciences, Královopolská 147, 612 64 Brno, Czech Republic.  
E-mail address: [konvalina@isibrno.cz](mailto:konvalina@isibrno.cz) (I. Konvalina).

sensitivity, nonconductivity, nano-sizes, and nanostructures, the characterization of many mesoporous metal oxides with high resolution by using common methods such as transmission electron microscopy (TEM) and scanning electron microscopy (SEM) often provides insufficient information [22,23]. This is because many imaging and spectroscopic techniques, especially those utilizing high energy beams (conventional SEM is usually operating from units of keV to 30 keV, TEM from tens of keV to 300 keV), damage the samples through various mechanisms [24]. Therefore, the development of new methods that allow for more precise imaging and analysis of the samples without damaging or altering them is essential to fully probe the structures as well as the properties of various nanomaterials. For example, the Schüth group did so for mesoporous silica using high resolution SEM operating at 10 keV and 30 kV [25]; however, the images are not of high quality due to the high voltage used to obtain higher resolution and the low current used to suppress sample damage. It should be also noted that the MacLachlan group did the observation of the structure in detail using helium ion microscopy (HIM) but such a tool is still not common (compared with SEM) [26].

Scanning low energy electron microscopy (SLEEM) is a technique that uses low energy electrons (below 1 keV) to image the native form of nanomaterials with high resolution [27,28]. As the low energy electrons constitute a low interaction volume as well as have an ability to eliminate charging at an identified critical energy (where the amounts of landed and emitted electrons are equal), SLEEM allows for detailed studies of the surface topography of nanomaterials. Furthermore, because it is gentle, less destructive, and yet sensitive to surfaces, SLEEM can produce higher resolution images of various nanomaterials even in their native forms. For the same reason, the samples being imaged with SLEEM are less susceptible to issues of electron beam-related structural damages and surface contamination, which are common in other SEM techniques. Note that, in conventional SEM lowering the electron dose can reduce sample damage associated with electron irradiation. The resulting image, however, will be noisier and of lower resolution. Decreasing the dose in any SEM will increase noise, but the resolution will not necessarily decrease. Despite many of its advantages and capabilities, though, SLEEM has not been used as much as SEM for analysis of nanomaterials such as mesoporous silicas.

In this report, we demonstrate that SLEEM can give super-resolution images of the native forms of mesostructured materials. We also show that the imaging can be done without producing noisy images. This “denoising” with low energy electrons is particularly effective when SLEEM is combined with advanced deep learning techniques. Deep learning is a machine learning technique that applies neural networks with many layers, allowing SLEEM to provide even more detailed images of the surface structures of materials. Such structural information is normally difficult to obtain or extract with standard SEM for materials like Au nanoparticles-loaded SBA-15 mesoporous silicas [29]. These nano-materials are chosen as model systems to demonstrate SLEEM’s capabilities because they possess inherent surface defects associated with their self-assembly synthesis and electron-beam sensitive metallic nanoparticles, and are thus difficult to clearly image by most conventional known methods [30]. Overall, the work demonstrates the potential applications of SLEEM and deep learning methods for advanced characterization of these materials to increase our understanding of their structures.

## 2. Materials and methods

### 2.1. Reagents and materials

A triblock copolymer, poly(ethylene glycol)-block-poly(propylene glycol)-block-poly(ethylene glycol) (Pluronic® P123, with average molecular weight of ~5800,) was obtained from BASF. Tetraethyl orthosilicate (TEOS), dichloromethane, toluene, sodium borohydride ( $\text{NaBH}_4$ ), 2-phenylethanethiol, hydrogen tetrachloroaurate(III) trihydrate ( $\text{HAuCl}_4 \cdot 3\text{H}_2\text{O}$ ), and diethyl ether were purchased from Sigma-

Aldrich. Hydrochloric acid (36.5 %) was received from Fischer Scientific. (3-Mercaptopropyl)trimethoxysilane (MPTS) was obtained from Gelest, Inc. Toluene (99.8 %), methanol (HPLC grade, 99.8 %), and tetra-n-octylammonium bromide were purchased from VWR. Ethanol (99.8 %) was received from Fluka. Deionized (DI) water was used for the synthesis of all materials.

### 2.2. Synthesis of Au nanoparticles-loaded SBA-15

To prepare Au-loaded SBA-15 mesoporous silica, which was used as a model system for the studies described herein [29], first, surfactant-extracted mesoporous SBA-15 (SBA-15) was synthesized as reported previously [31,32]. Typically a solution containing P123, HCl, TEOS, and  $\text{H}_2\text{O}$  in a mass ratio of 2 : 12 : 4.3 : 52, respectively, as prepared. This was done by mixing P123, HCl, and  $\text{H}_2\text{O}$ , and then stirring the solution at 40 °C for 5 min. After adding TEOS, the solution was stirred at 40 °C for 24 h. The solution was then aged at 65 °C for 24 h. The solution was filtered, and the solid product was washed with copious amount of water and dried in air. The resulting surfactant-containing SBA-15 (4 g) was taken and stirred in a solution composed of ethanol (400 mL) and diethyl ether (400 mL) at 50 °C for 5 h to remove the surfactant (or P123) templates in it. The solid product was separated by filtration and dried in oven at 40 °C for 2 h. This gave surfactant-extracted mesoporous silica, SBA-15. Then, SBA-15 sample (500 mg) was stirred with MPTS (0.64 mL, 3.68 mmol) in toluene at 80 °C for 6 h. The mixture was filtered. The solid material was quickly washed with toluene (3 × 20 mL) and then with ethanol (3 × 20 mL) and air-dried. This gave 3-mercaptopropyl-functionalized SBA-15, which was named SBA-15-SH.

Monolayer-protected Au nanoparticles were synthesized as reported previously [29,33]. In a three-neck round-bottom flask,  $\text{HAuCl}_4 \cdot 3\text{H}_2\text{O}$  (1.55 g, 3.94 mmol) was dissolved in water (50 mL). Toluene (100 mL) and tetra-n-octylammonium bromide (2.56 g, 4.68 mmol) were added into the solution while stirring. After vigorous stirring of the biphasic mixture for 30 min, the dark-red organic phase was separated and cooled to 0–2 °C using an ice bath. Into the solution under slow stirring, 2-phenylethanethiol (2.6 mL, 19.4 mmol) was added. The solution turned light yellow quickly, and then opaque white after 1.5 h. After this,  $\text{NaBH}_4$  (1.89 g, 50.0 mmol) dissolved in ice-cold DI water (30 mL) was added into the solution under vigorous stirring. The resulting black solution was stirred at room temperature for 24 h. The organic phase was separated with a separatory funnel and washed with 50 mL water, three times. Toluene was then evaporated under reduced pressure yielding a black product. Residual 2-phenylethanethiol in the crude product was removed with methanol (200 mL). After 4 h, the supernatant was discarded, and the solid product was re-dispersed in methanol (200 mL) and left in a fridge overnight. This step was repeated three times. Finally, a crystalline black powder material consisting of pure  $\text{Au}_{144}(\text{SCH}_2\text{CH}_2\text{Ph})_{60}$  was obtained.

The next step involved mixing a solution of  $\text{Au}_{144}(\text{SCH}_2\text{CH}_2\text{Ph})_{60}$  in dichloromethane (2  $\mu\text{M}$ ) with SBA-15-SH (300 mg) dispersed in dichloromethane (30 mL). The mixture was stirred at room temperature for 3 h. The solution was centrifuged, and the residue was washed with dichloromethane (10 mL) three times (via sonication, centrifugation, and decantation). The resulting solid material was air-dried to finally give Au-loaded SBA-15, which was also called SBA-15-SH-Au<sub>144</sub>. The immobilization of Au nanoparticles into SBA-15-SH was qualitatively confirmed by the change of the white color of the SBA-15-SH sample into purple/red.

### 2.3. Imaging with SLEEM

At low landing electron beam operation, SEM using deceleration of the electron beam could improve resolution and contrast. SLEEM uses a cathode lens system to decelerate the electron beam. Beam deceleration is a relatively simple method that can also be applied in SLEEM to reduce

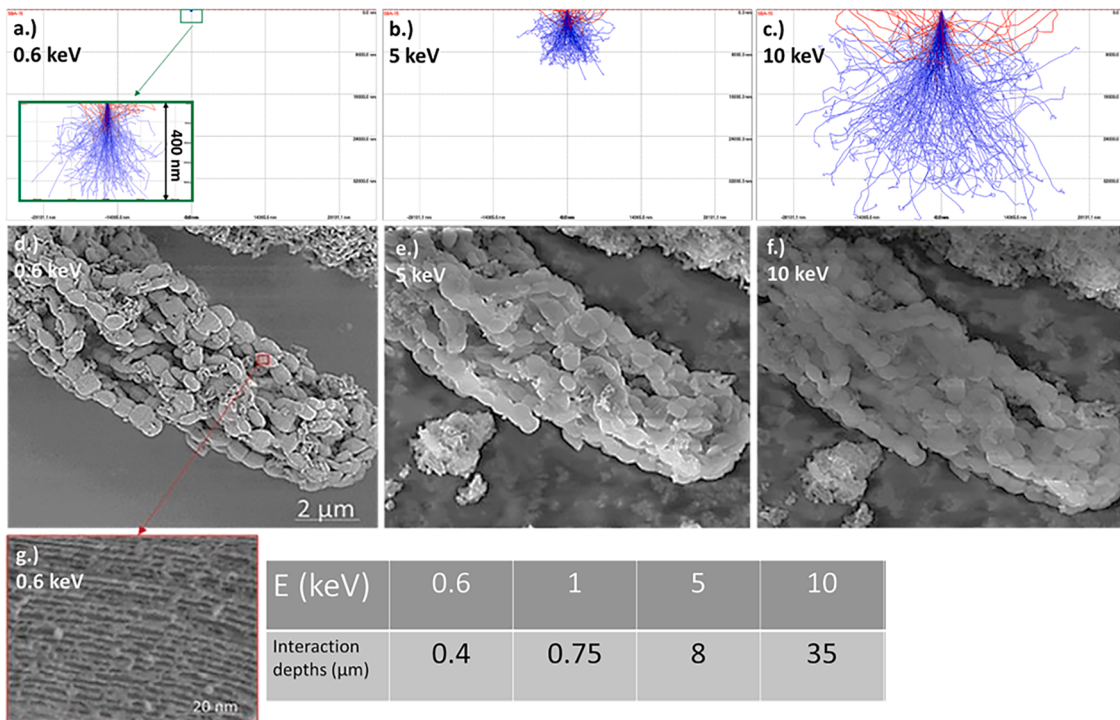


**Fig. 1.** a.) – c.) Monte Carlo simulations of the interaction depths within SBA-15 mesoporous material (Au particles are not included in the simulations and the material density used for the simulation  $0.067 \text{ g/cm}^3$  [ACS Material®]) when the sample is exposed to low energy electron beams in SLEEM with landing energies of 0.6 keV, 5 keV, and 10 keV (CASINO®, <https://doi.org/10.1002/sca.20000>). The red paths are of those backscattered electrons (BSEs) that have left the sample. d.) – f.) The corresponding SLEEM images obtained with these landing electron beams. h.) The interaction depths of energy electrons with the sample upon its exposure to selected energies of landing electron beams are summarized in the presented table.

electron beam energy and to improve imaging parameters, such as resolution and contrast simultaneously. It should be noted that in the SLEEM mode we acquire a mixture of secondary electrons (SEs) and backscattered electrons (BSEs) signals, so the BSE contribution to the higher contrast observed becomes questionable. Unfortunately, the lower interaction volume of low energy electrons can mean higher electron density (thanks the higher yield of SEs) in the area imaged. If the sample is very sensitive to electron beams, it can still suffer from electron beam-related contamination or damage, making its imaging in high resolution difficult.

SLEEM studies were carried out with an electron microscope equipped with a cathode lens and transmission mode (or a low voltage scanning transmission electron microscope (LV-STEM)). The instrument is XHR S(T)EM Magellan 400 microscope (FEI®), and it can operate with low energy electrons. Its cathode lens system allowed the observation of samples at a chosen landing energy of primary electrons. The operation of the microscope at low beam energies can offer several advantages, including an improvement in the contrast of the images of the samples by lowering the beam energy, suppression of noise (higher signal of detected electrons), more localized beam-specimen interactions (or smaller interaction volumes), weaker artifacts due to charging, reduced edge effect, and improved crystal orientation-related contrast with crystalline samples [34–37].

#### 2.4. Deep learning

The deep learning we applied is based on machine learning method that combines VGG Convolutional Neural Networks (CNNs) [38] and Generative Adversarial Networks [39]. It is inspired by the SRGAN architecture [40]. The neural network model is trained to upscale images by the factor of four on a huge general-purpose dataset DIV2K [4], and then finetuned on our data set of microscopy images. The model consists of two sub-models: (i) a generator, which encodes low-resolution

images and then up-sample their sizes, and (ii) a discriminator, which is trained to differentiate between super-resolution images and original photo-realistic images. In contrast to conventional neural network models, which are trained to optimize a single loss function, we used a weighted sum of two loss functions, namely (i) content loss that is motivated by the perceptual similarity and (ii) adversarial loss that reflects the classification error of the discriminator.

##### 2.4.1. The generator network

The generator network takes a low-resolution image as input and aims to produce a corresponding high-resolution image. It employs a deep CNN architecture with multiple convolutional layers to learn the mapping between the low-resolution and high-resolution image spaces. The input to the generator is the low-resolution image, represented as a tensor of size  $(W, H, C)$ , where  $W$  and  $H$  are the width and height of the image, and  $C$  is the number of channels. The number of channels is 1 in our case.

A series of convolutional layers are employed to capture low-level features in the input image. These layers consist of  $3 \times 3$  filters with a stride of 1 and use rectified linear unit (ReLU) activation functions to introduce non-linearity. The generator network utilizes residual learning to handle the difficulty of training deep networks. It employs a stack of residual blocks, where each block consists of two convolutional layers with  $3 \times 3$  filters. Batch normalization is applied after each convolutional layer, and skip connections are used to directly propagate information from the input to the output of each residual block.

To increase the resolution of the image, up-sampling layers are used. These layers convert low-resolution feature maps into high-resolution feature maps by rearranging the pixels. The final layer of the generator network generates the high-resolution output image. It employs a convolutional layer with  $3 \times 3$  filters and a tanh activation function to produce pixel values in the range  $[-1, 1]$ .

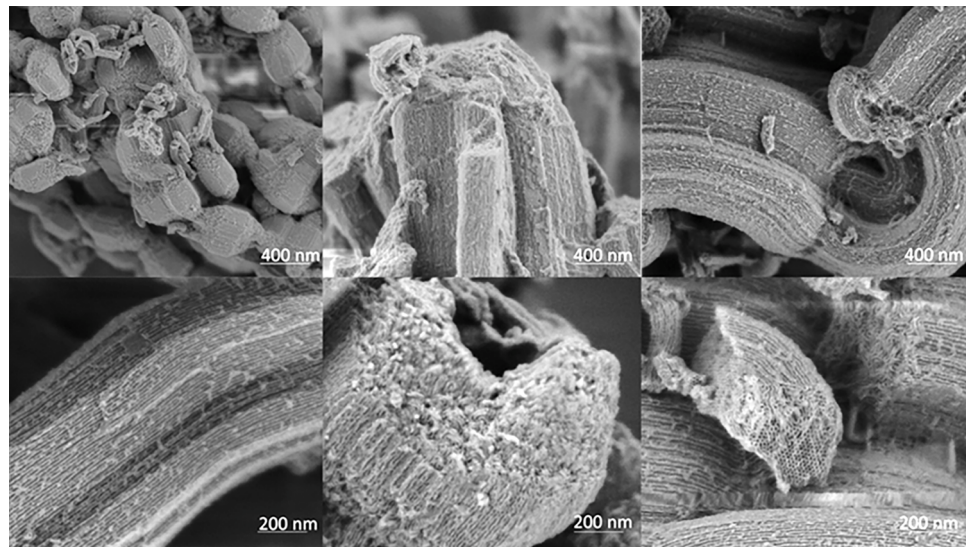


**Fig. 2.** Selected imaged areas of Au-loaded mesoporous silica by SLEEM operating with 0.6 keV energy electron beam.

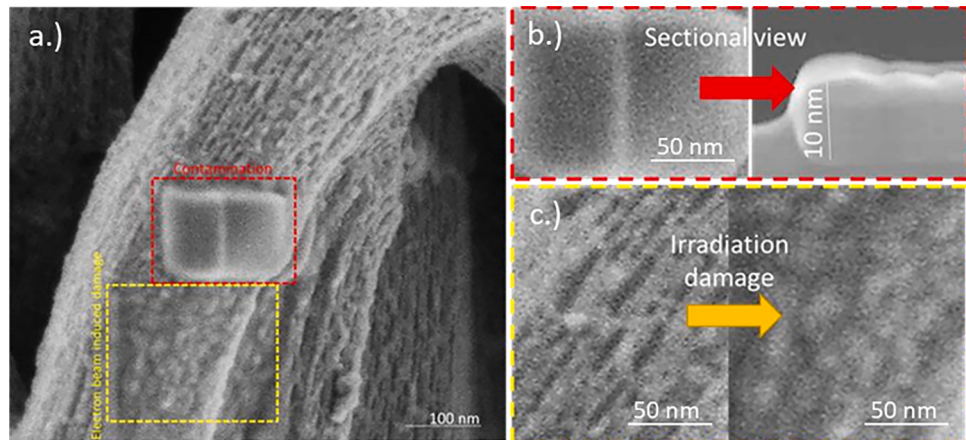


**Fig. 3.** The possible negative effects of electron beam irradiation on Au-loaded SBA-15 mesoporous silica during its imaging are shown. The figure shows SLEEM images taken after irradiation of the sample with 2 keV electron beam (b.) and 30 keV electron beam (c.). The red boxes (b.) display how a longer irradiation time with 2 keV electron beam causes contamination of the sample whereas the yellow boxes show how a higher electron dose ( $2 \text{ C}/\text{cm}^2$ ) causes also irradiation damage on the structures of mesoporous silica sample.

#### 2.4.2. The discriminator network

The discriminator network is responsible for distinguishing between the generated high-resolution images and the real high-resolution images. It is designed as a CNN classifier that takes an image as input and outputs a probability indicating whether the image is real or generated.

The input to the discriminator is either a real high-resolution image or a generated high-resolution image. The discriminator network consists of multiple convolutional layers with  $3 \times 3$  filters and a stride of 1. Each convolutional layer is followed by batch normalization and a LeakyReLU activation function. The convolutional layers help the discriminator extract features from the input image, capturing both low-level and high-level information. A global pooling layer is employed to aggregate the extracted features into a fixed-length vector representation. It averages the feature maps along the spatial dimensions. The global pooling layer is connected to a series of fully connected layers, which progressively reduce the dimensionality of the features. The final layer of the discriminator network is a single sigmoid unit that outputs a probability value between 0 and 1, indicating the likelihood that the input image is real.

#### 2.4.3. Training

The model is trained in an adversarial manner, where the generator and discriminator networks are trained alternately to improve their performances. The generator aims to generate high-resolution images that can fool the discriminator, while the discriminator aims to accurately distinguish between real and generated images. The training process involves minimizing two main objectives: the content loss and the adversarial loss. The content loss measures the similarity between the generated and ground truth high-resolution images, computed using mean squared error (MSE) on VGG network features. The adversarial loss encourages the generator to generate more realistic images by minimizing the binary cross-entropy loss between the discriminator's predictions and the true labels.

### 3. Results and discussion

#### 3.1. Surface sensitivity, interaction depth, and images of samples under low voltage electron beams

The material used as a model system for the studies described herein is synthesized using previously published methods [3,29]. It is

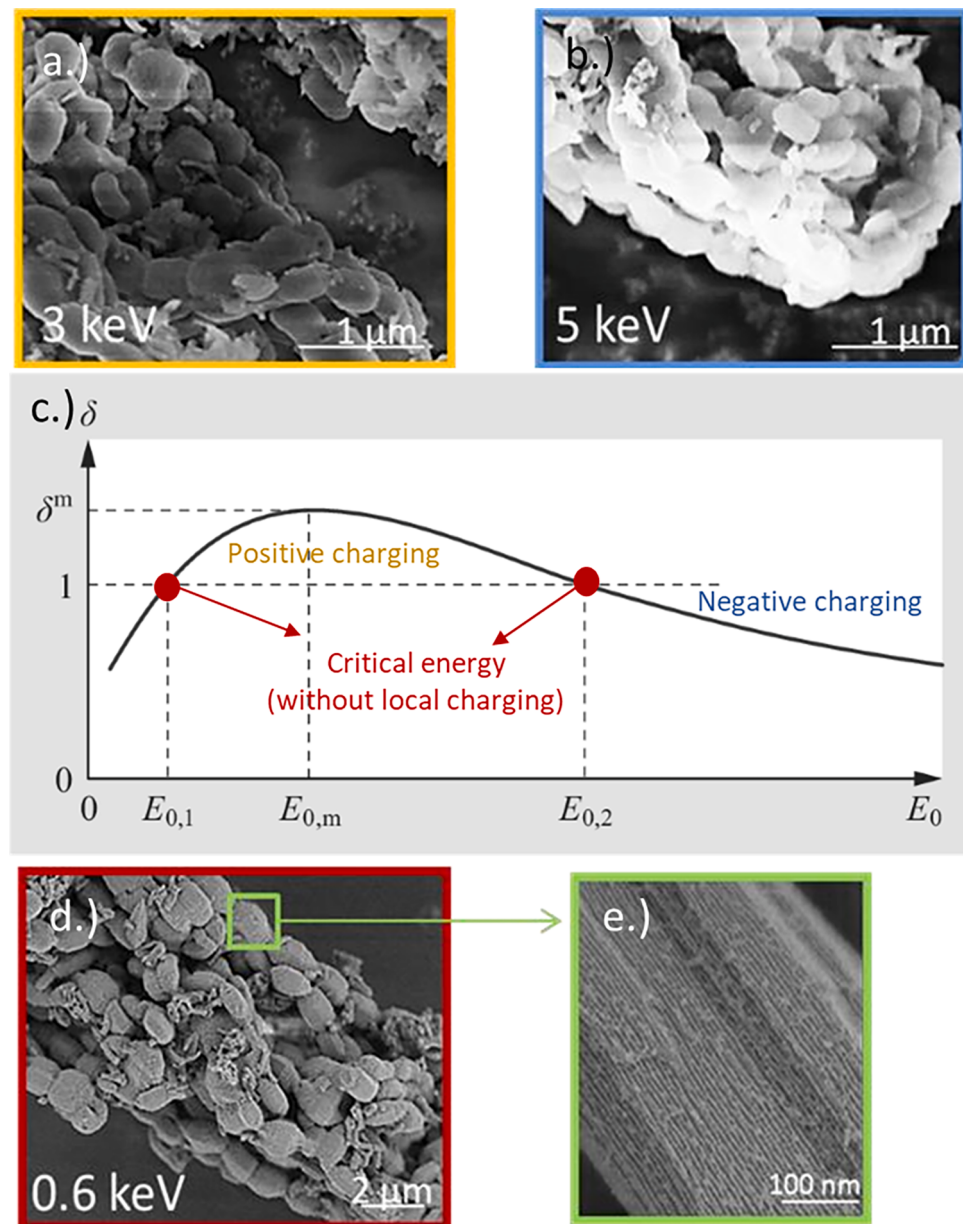


**Fig. 4.** SLEEM images taken with different slow energy electron beams. Depending on the beam energy, positive charging, negative charging, or no charging may occur. In the first two cases, the images are blurred. However, in the last case, where 0.6 keV electron beam is used, the image is clearer (c.)). This is achieved by choosing the electron beam as 0.6 keV at which positive charging and negative charging balance out. Note that such clear surface images are difficult to obtain for materials such as mesoporous silicas using conventional techniques, including SEM and STEM.

composed of mesoporous silica structures with Au nanoparticles, with diameters of approximately from 1 nm to 5 nm. Its other structural features have been reported in detail before [29]. Notably, its standard TEM images reveal the presence of nanoparticles that appear to be on the surfaces of the material while some could actually be inside the pores of the material, as described further below. Furthermore, possible necking and agglomeration of the particles due to the relatively high electron beam emitted by a standard TEM could not be ruled out. In fact, conventional microscopy images (conventional SEM is usually operating from units to 30 keV, TEM from tens to 300 keV) that we and others had previously reported for various nanoparticles-loaded mesoporous silica materials indicated so [41–43].

Thus, we have set out an experiment using SLEEM to determine the benefits it may have to explore such nanostructured materials using Au-SBA-15 as a model system. It is worth noting that the energies of the electron beams used in SLEEM are much lower than those typically used

in conventional electron microscopes. Just for illustration (in the simulations the Au nanoparticles are not included and also SE trajectories are not presented), Fig. 1 shows the Monte Carlo simulations (<https://doi.org/10.1002/sca.20000>) of the interaction volumes of SLEEM's electron beams in mesoporous silica when electron beams with landing energies of 0.6 keV, 5 keV, and 10 keV are applied. The possible trajectories of the BSEs are also included in the simulations. As can be seen in Fig. 1, the interaction depth exponentially decreases as the energy of the landing electrons decreases, which is true until 20 keV. It is worth noting that lower interaction depth and volume can produce greater surface sensitivity, allowing for the observation of the structure of the sample in more detail, especially in the case of porous materials. This is evidenced with the actual SEM images obtained for the sample with these low energy beams, which are depicted in the Fig. 1. The interaction depths of electrons with the sample for different selected low electron landing energies are summarized in the table presented in Fig. 1

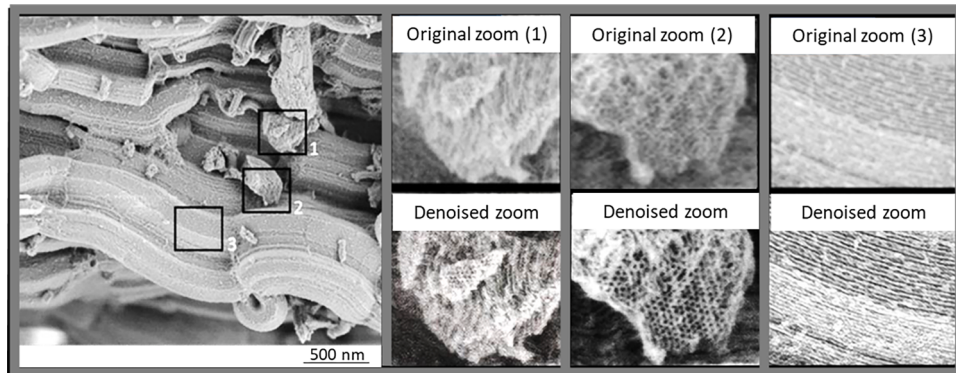


**Fig. 5.** SLEEM images supported by deep learning, showing selected details before and after “denoising” and also image sharpness/resolution improvement.. The latter images show a much better resolution, demonstrating the advantages of deep learning (or SLEEM + deep learning).

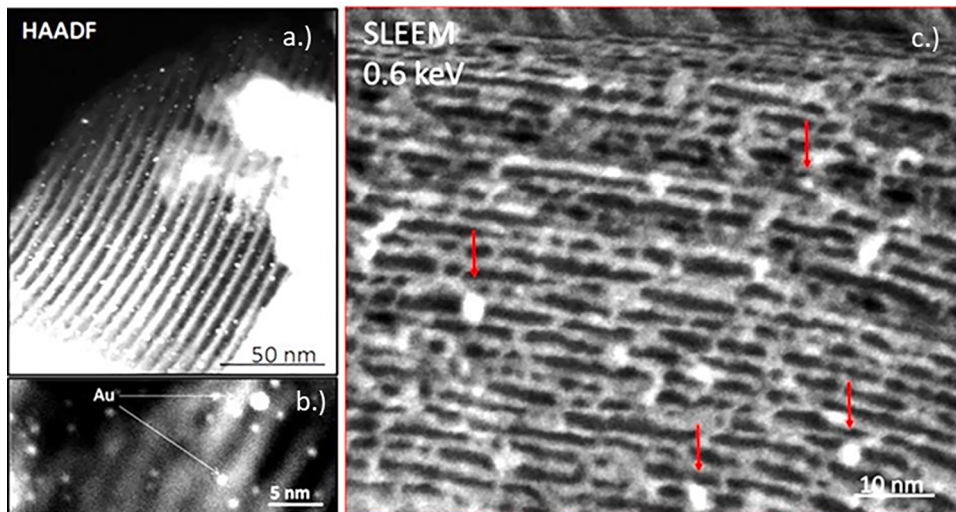


**Fig. 6.** (a.) and b.)) Traditional HR STEM images obtained with 30 keV versus (c.) an ultra-high resolution image obtained with SLEEM with 0.6 keV electron beam combined with deep learning method for Au nanoparticles-loaded SBA-15 meso-porous silica are compared.

as well.

The images of mesoporous materials obtained using SLEEM with energy beams of 0.6 keV, 5 keV, and 10 keV indicate that the one taken with 0.6 keV is the clearest. Conversely, it can be said that 0.6 keV produces the clearest images for these materials. The charging measurements are described in detail in section 3.2 below. The higher beams lead to lower surface sensitivity and cause also electrostatic charging in the sample. Mesoporous silica generally charges during electron microscopy imaging due to non-conductive character. Massive charging is particularly observed when the material is imaged with electron beams below 0.6 keV. Hence, energy beams below 0.6 keV cannot be viably used to image this material. Additional SLEEM images obtained with the optimal slow electrons with energy of 0.6 keV are shown in Fig. 2.

In conventional electron microscopy, when higher resolution images are sought, more electron dose is often applied; however, this can also damage the samples and cause artifacts due to irradiation-related contamination [41–43]. This conundrum is more pronounced especially when higher resolution and structurally detailed images of a sample are needed, which will naturally require an application of greater beam dose and longer imaging times. The issue is even much more prominent for beam-sensitive samples like Au-loaded mesoporous silica, as can be seen in the results we have obtained with higher energy electron beam in Fig. 3. While higher energy electron beam naturally causes contamination of the sample by polymerization of some surface adsorbed hydrocarbons, high current and long imaging times can lead to

direct damage of the samples (this also means that changes in the structures of the materials can be observed during imaging due to these effects). This is also why we have intentionally chosen this particular material as a model system herein to study it with low energy electrons to show their beneficial advantages for imaging.

If contamination exists or if the sample is sensitive to irradiation, nanoparticles with size below 5 nm are difficult to image and sectional views of porous structures with good resolution are impossible to get, as can be seen in Fig. 3b.) and c.). Making the scanning very fast does not provide sufficiently meaningful information either. However, in this work, we also show that this imaging problem in microscopy can be resolved by using advanced deep learning technique, as presented in Section 3.3. below.

### 3.2. Charging

The charging effects caused by the non-conductive character of mesoporous silica sample can be mitigated with SLEEM by operating it at a so-called “critical energy”, where the number of impacted electrons and emitted electrons are equal. Under this condition, overall specimen charging is neutral and clearer images can be obtained. Furthermore, the potential at the sample is steady. As can be seen in Fig. 4a.) b.) and d.), the total electron yield  $\sigma$  (y axis) during imaging a sample can be positive, negative, or zero. It is zero if the amounts of impacted electrons and emitted electrons are equal. One of the most important advantages of

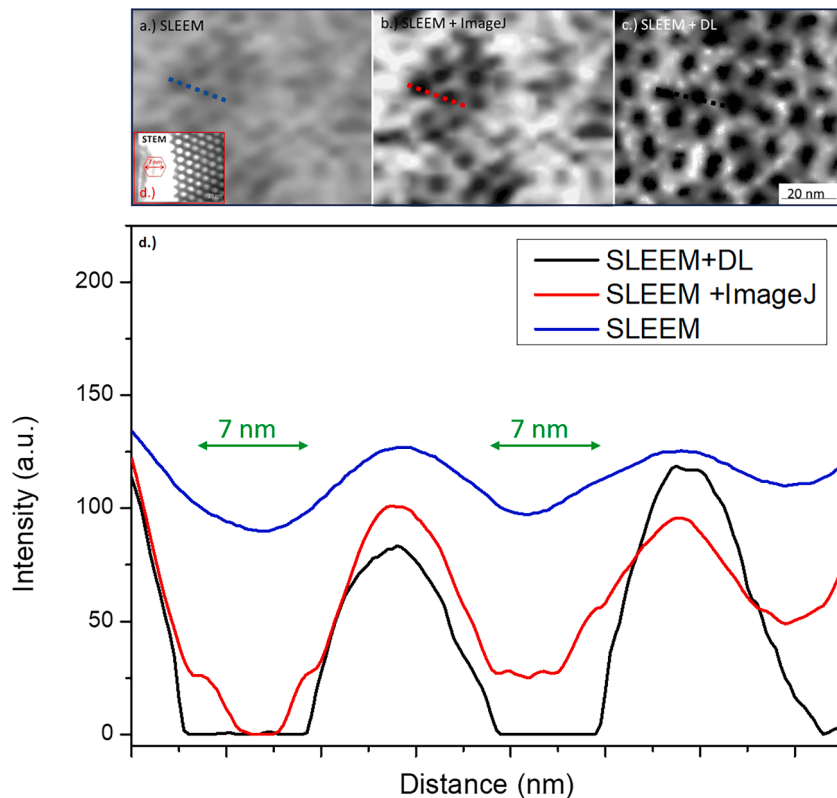


**Fig. 7.** Comparison of cross-sectional SLEEM image obtained with 0.6 keV electron beam (a.) and SLEEM image improved with ImageJ program (b.) versus cross-sectional deep learning-enhanced SLEEM image (c.) of Au-loaded SBA-15. The structure observed by STEM (d.) is also highlighted. The graph of the line profiles (highlighted in the images) presents increasing dynamic range which is important for the structural size measurements.

SLEEM technique is the ability to choose an optimal electron beam energy to create equal number of impacted and emitted electrons. This, in turn, helps avoid charging (both positive and negative charging, which are shown in yellow and blue, respectively, in Fig. 4). The positions where  $\sigma$  is 1 are marked with  $E_{0,1}$  and  $E_{0,2}$  in Fig. 4, and they represent the desirable critical energies of SLEEM to image the sample. Imaging the sample at either of these two electron beam energies causes no local charging, giving clearer images. For our samples we selected the lower critical energy (0.6 keV) due to their higher surface sensitivity, which is necessary for the observation of the sample in detail.

### 3.3. Deep learning to improve SLEEM images (contrast and resolution)

In this work, we also demonstrate that the quality of the SLEEM images can be improved further by introducing deep learning. This method has never been applied to electron microscope images of mesoporous materials before, to the best of our knowledge. The quality of the image can be improved, with an advanced deep learning method. In other words, the SLEEM images can be further augmented and higher resolution observation of the structures of the materials can be achieved by applying deep learning (neural networks) to the SLEEM images. This is demonstrated in Fig. 5, which shows detailed (or high resolution) images with “denoising” via deep learning. While the original images are blurred, those obtained after denoising show clearer corrugated structures and pores on the surfaces of the mesoporous materials. These images illustrate the advantage of performing “denoising” through deep learning or the ability of machine learning to obtain clearer structural features of materials that could not have been observed otherwise. Thus, high-resolution SEM imaging of samples in beam deceleration mode with increased contrast and resolution could be attained by using SLEEM equipped with a cathode lens system and by applying deep learning (neural networks).

Importantly also, higher resolution (pixel count is increased and signal to noise ratio is increased as well) and enhanced contrast are preserved in the denoised SLEEM images, as presented in Fig. 6. It is evident that the denoised SLEEM images obtained with 0.6 keV electron beam, coupled with deep learning, for Au nanoparticles-loaded mesoporous silica show 3-D like structures and the locations of the Au nanoparticles. It also shows where exactly the nanoparticles, below 5 nm in size, are within the material, in higher resolution and contrast compared with those obtained HR STEM images (Fig. 6). The HR STEM images in HAADF segment, displayed for comparison, do not clearly depict the actual location of the Au nanoparticles in the Au nanoparticles-loaded SBA-15 sample. In other words, the HR STEM images, show 2-D like structures as if the nanoparticles are on the surfaces of the mesoporous silica despite some that are present within the channel pores. Thus, the deep learning technique combined with SLEEM can dig out information about the overall structures of the samples better than conventional SEM does.

In addition, SLEEM in combination with deep learning technique allows for the observation of surface nanoporous structures more clearly, as can be seen in the comparative SLEEM image, SLEEM image that is simply improved with ImageJ program (*ImageJ*, U. S. National Institutes of Health, Bethesda, Maryland, USA, <https://imagej.nih.gov/ij/>, 1997–2018) (brightness/contrast, process – sharpen), and STEM images of Au nanoparticles-loaded SBA-15 (Fig. 7). The final SLEEM+DL image (Fig. 7 c.) of the material shows corrugated structures and rough surfaces. The corresponding STEM images, however, show as if the material has smooth and well-ordered honeycomb surface structure. Many STEM and TEM images reported before displayed similar smooth surface structures for such materials [29,42,44] even though they actually are not, as can be seen in their SLEEM images.

As a final note, it is worth noting that the imaging methods reported herein are also comparable (in terms of ultra-high resolution, superb



- [26] A.S. Terpstra, K.E. Shopsowitz, C.F. Gregory, A.P. Manning, C.A. Michal, W. Y. Hamad, J. Yang, M.J. MacLachlan, Helium ion microscopy: a new tool for imaging novel mesoporous silica and organosilica materials, *Chem. Comm.* 49 (16) (2013) 1645–1647, <https://doi.org/10.1039/C3CC38569H>.
- [27] D. Phifer, L. Tuma, T. Vystavel, P. Wandrol, R. Young, Improving SEM imaging performance using beam deceleration, *Micros. Today* 17 (4) (2009) 40–49, <https://doi.org/10.1017/S1551929509000170>.
- [28] L. Frank, M. Hovorka, Š. Mikmeková, E. Mikmeková, I. Müllerová, Z. Pokorná, Scanning electron microscopy with samples in an electric field, *Materials (Basel)* 5 (12) (2012) 2731–2756, <https://doi.org/10.3390/ma5122731>.
- [29] S. Das, A. Goswami, M. Hesari, J.F. AlSharab, E. Mikmeková, F. Maran, T. Asefa, Reductive deprotection of monolayer protected nanoclusters: an efficient route to supported ultrasmall Au nanocatalysts for selective oxidation, *Small* 10 (8) (2014) 1473–1478, <https://doi.org/10.1002/smll.201302854>.
- [30] H.W. Hillhouse, J.W. van Egmond, M. Tsapatsis, J.C. Hanson, J.Z. Larese, Synthesis and characterization of ordered arrays of topological defects in mesoporous silica films, *Chem. Mater.* 12 (10) (2000) 2888–2893, <https://doi.org/10.1021/cm000425k>.
- [31] D. Zhao, J. Feng, Q. Huo, N. Melosh, G.H. Fredrickson, B.F. Chmelka, G.D. Stucky, Triblock copolymer syntheses of mesoporous silica with periodic 50 to 300 angstrom pores, *Science* 279 (5350) (1998) 548–552, <https://doi.org/10.1126/science.279.5350.548>.
- [32] M. Brust, M. Walker, D. Bethell, D.J. Schiffrin, R. Whymann, Synthesis of thiol-derivatised gold nanoparticles in a two-phase liquid–liquid system, *J. Chem. Soc., Chem. Commun.* (7) (1994) 801–802, <https://doi.org/10.1039/C39940000801>, 1994.
- [33] R.L. Donkers, D. Lee, R.W. Murray, Synthesis and isolation of the molecule-like cluster Au38 (PhCH<sub>2</sub>CH<sub>2</sub>S)<sub>24</sub>, *Langmuir* 20 (5) (2004) 1945–1952, <https://doi.org/10.1021/la035706w>.
- [34] I. Müllerová, M. Hovorka, F. Mika, E. Mikmeková, Š. Mikmeková, Z. Pokorná, L. Frank, Very low energy scanning electron microscopy in nanotechnology, *Int. J. Nanotechnol.* 9 (8–9) (2012) 695–716, <https://doi.org/10.1504/IJNT.2012.046749>.
- [35] E.M. Mikmeková, I. Müllerová, L. Frank, A. Paták, J. Polcák, S. Sluyterman, M. Lejeune, I. Konvalina, Low-energy electron microscopy of graphene outside UHV: electron-induced removal of PMMA residues used for graphene transfer, *J. Electron Spectrosc. Relat. Phenomena* 241 (2020) 146873, <https://doi.org/10.1016/j.elspec.2019.06.005>.
- [36] I. Müllerová, E. Mikmeková, Š. Mikmeková, I. Konvalina, L. Frank, Practical use of scanning low energy electron microscope (SLEEM), *Microsc. Microanal.* 22 (S3) (2016) 1650–1651, <https://doi.org/10.1017/S1431927616009090>.
- [37] E.M. Mikmeková, I. Konvalina, I. Müllerová, M. Lejeune, T. Asefa, Treatment and observation of advanced carbon-based nanomaterials by slow electrons, *Microsc. Microanal.* 26 (S2) (2020) 2682–2684, <https://doi.org/10.1017/S1431927620022412>.
- [38] K. Simonyan, A. Zisserman, Very deep convolutional networks for large-scale image recognition, *arXiv preprint arXiv:1409.1556* (2014). <https://doi.org/10.48550/arXiv.1409.1556>.
- [39] I. Goodfellow, J. Pouget-Abadie, M. Mirza, B. Xu, D. Warde-Farley, S. Ozair, A. Courville, Y. Bengio, Generative adversarial networks, *Commun. ACM* 63 (11) (2020) 139–144, <https://doi.org/10.1145/3422622>.
- [40] C. Ledig, L. Theis, F. Huszár, J. Caballero, A. Cunningham, A. Acosta, A. Aitken, A. Tejani, J. Totz, Z. Wang, W.S. Twitter, Photo-realistic single image super-resolution using a generative adversarial network, *arXiv:1609.04802 [cs.CV]* (2017). <https://doi.org/10.48550/arXiv.1609.04802>.
- [41] W. Albrecht, A. van de Glind, H. Yoshida, Y. Isozaki, A. Imhof, A. van Blaaderen, P. E. de Jongh, K.P. de Jong, J. Zečević, S. Takeda, Impact of the electron beam on the thermal stability of gold nanorods studied by environmental transmission electron microscopy, *Ultramicroscopy* 193 (2018) 97–103, <https://doi.org/10.1016/j.ultramic.2018.05.006>.
- [42] Y. Liu, Y. Sun, Electron beam induced evolution in Au, Ag, and interfaced heterogeneous Au/Ag nanoparticles, *Nanoscale* 7 (32) (2015) 13687–13693, <https://doi.org/10.1039/C5NR03523F>.
- [43] Z. Liu, R. Che, A.A. Elzatahry, D. Zhao, Direct imaging Au nanoparticle migration inside mesoporous silica channels, *ACS Nano* 8 (10) (2014) 10455–10460, <https://doi.org/10.1021/nn503794v>.
- [44] Y. Guaré, C. Thieuleux, A. Mehdi, C. Reyé, R.J. Corriu, S. Gomez-Gallardo, K. Philippot, B. Chaudret, In situ formation of gold nanoparticles within thiol functionalized HMS-C16 and SBA-15 type materials via an organometallic two-step approach, *Chem. Mater.* 15 (10) (2003) 2017–2024, <https://doi.org/10.1021/cm0213218>.
- [45] A.S. Terpstra, K.E. Shopsowitz, G.F. Camille, A.P. Manning, C.A. Michal, W. Y. Hamad, J. Yang, M.J. MacLachlan, Helium ion microscopy: a new tool for imaging novel mesoporous silica and organosilica materials, *Chemical Commun.* 49 (16) (2013), <https://doi.org/10.1039/C3CC38569H>, 1645–